Elastic Torque and the Levitation of Metal Wires by a Nematic Liquid Crystal

C. Lapointe, *et al.*

Science **303**, 652 (2004);
DOI: 10.1126/science.1092608

Science (print ISSN 0036-8075; online ISSN 1095-9203) is published weekly, except the last week in December, by the American Association for the Advancement of Science, 1200 New York Avenue NW, Washington, DC 20005.

evidence for live ^{99}Tc in the early solar system is therefore small.

References and Notes

1. R. S. Lewis, M. Tang, J. F. Wacker, E. Anders, E. Steel, *Nature* **326**, 160 (1987).
2. T. Bernatowicz *et al*., *Nature* **330**, 728 (1987).
3. E. Zinner, *Meteorit. Planet. Sci.* **33**, 549 (1998).
4. S. Amari, P. Hoppe, E. Zinner, R. S. Lewis, *Meteoritics* **30**, 679 (1995).
5. P. Hoppe, U. Ott, in *Astrophysical Implications of the Laboratory Study of Presolar Materials,* T. J. Bernatowicz, E. Zinner, Eds. (American Institute of Physics, Woodbury, NY, 1996), pp. 27–58.
6. B. S. Meyer, *Annu. Rev. Astron. Astrophys.* **32**, 153 (1994).
7. G. K. Nicolussi *et al*., *Science* **277**, 1281 (1997).
8. G. K. Nicolussi *et al*., *Geochim. Cosmochim. Acta* **62**, 1093 (1998).
9. G. K. Nicolussi *et al*., *Phys. Rev. Lett.* **81**, 3583 (1998).
10. M. R. Savina *et al*., *Geochim. Cosmochim. Acta* **67**, 3201 (2003).
11. M. Lugaro *et al*., *Astrophys. J.* **593**, 486 (2003).
12. P. W. Merrill, *Astrophys. J.* **116**, 21 (1952).
13. S. J. Little, I. R. Little-Marenin, W. H. Bauer, *Astron. J.* **94**, 981 (1987).
14. V. V. Smith, D. L. Lambert, *Astrophys. J.* **311**, 843 (1986).
15. H. Poths, S. Schmitt-Strecker, F. Begemann, *Geochim. Cosmochim. Acta* **51**, 1143 (1987).
16. I. D. Hutcheon, J. T. Armstrong, G. J. Wasserburg, *Geochim. Cosmochim. Acta* **51**, 3175 (1987).
17. H. Becker, R. J. Walker, *Chem. Geol.* **196**, 43 (2003).
18. J. H. Chen, D. A. Papanastassiou, G. J. Wasserburg, *Lunar Planet. Sci.* **XXXIV**, 1789 (2003).
19. P. Hoppe, S. Amari, E. Zinner, T. Ireland, R. S. Lewis, *Astrophys. J.* **430**, 870 (1994).
20. S. Amari, R. S. Lewis, E. Anders, *Geochim. Cosmochim. Acta* **58**, 459 (1994).
21. Z. Ma, R. N. Thompson, K. R. Lykke, M. J. Pellin, A. M. Davis, *Rev. Sci. Instrum.* **66**, 3168 (1995).
22. M. R. Savina *et al*., *Geochim. Cosmochim. Acta* **67**, 3215 (2003).
23. R. Gallino *et al*., *Astrophys. J.* **497**, 388 (1998).
24. C. Arlandini *et al*., *Astrophys. J.* **525**, 886 (1999).
25. Z. Y. Bao *et al*., *Atom. Data Nucl. Data Tables* **76**, 70 (2000).
26. In our model, each ^{13}C pocket gives rise to a unique G-component; however, they are all the same within 5‰, so we compare our data to the average. The Ru G-component is not at δ^{104}Ru = –1000‰, corresponding to no ^{104}Ru at all, because a small amount of ^{104}Ru is produced by bridging ^{103}Ru, whose 39-day half-life is long enough to permit a few captures during the *s*-process neutron exposure (see Fig. 1).
27. F. Voss, K. Wisshak, K. Guber, F. Käppeler, G. Reffo, *Phys. Rev. C* **50**, 2582 (1994).
28. K. Takahashi, K. Yokoi, *Atom. Data Nucl. Data Tables* **36**, 375 (1987).
29. B. Fegley, K. Lodders, H. Palme, *Meteoritics* **28**, 346 (1993).
30. Y. Kashiv, personal communication.
31. G. J. Wasserburg, M. Busso, R. Gallino, C. M. Raiteri, *Astrophys. J.* **424**, 412 (1994).
32. J. H. Williamson, *Can. J. Phys.* **46**, 1845 (1968).

33. We thank R. N. Clayton, L. Nittler, and two anonymous reviewers for careful reading of this paper. Supported by the U.S. Department of Energy, Basic Energy Sciences–Material Sciences under contract W-31-109-ENG-38; NASA grants 8336 (S.A.), 9510 (A.M.D.), and an unnumbered grant (M.J.P.); the University of Chicago; and the Italian FIRB Progetto Origine Astrofisica degli Elementi Pesanti Oltre il Ferro. The University of Chicago operates Argonne National Laboratory under contract with the U.S. Department of Energy.

Supporting Online Material

www.sciencemag.org/cgi/content/full/303/5658/649/DC1
Table S1

28 July 2003; accepted 2 December 2003

Elastic Torque and the Levitation of Metal Wires by a Nematic Liquid Crystal

C. Lapointe, A. Hultgren, D. M. Silevitch, E. J. Felton, D. H. Reich, R. L. Leheny

Anisotropic particles suspended in a nematic liquid crystal disturb the alignment of the liquid crystal molecules and experience small forces that depend on the particles' orientation. We have measured these forces using magnetic nanowires. The torque on a wire and its orientation-dependent repulsion from a flat surface are quantitatively consistent with theoretical predictions based on the elastic properties of the liquid crystal. These forces can also be used to manipulate submicrometer-scale particles. We show that controlled spatial variations in the liquid crystal's alignment convert the torque on a wire to a translational force that levitates the wire to a specified height.

Complex fluids are soft materials that have liquid-like properties but differ from ordinary liquids because of internal structure on the nanometer or micrometer scale. The classic example of a complex fluid is a polymer solution containing long chain-like molecules whose presence alters the flow behavior. Complex fluids are ubiquitous; they occur, for example, in living organisms and in many important technologies. When particles are suspended in a complex fluid, effects from entropy, interfacial phenomena, or other sources can generate forces on the particles that are not present in ordinary liquids (*1*). Understanding and controlling these forces are important scientific challenges. For example, the emergent technique of microrheology uses the motion of small particles in a complex fluid to uncover characteristics of the fluid at length scales and time scales that are inaccessible to bulk probes (*2*). The relations between the forces that give rise to this motion and the intrinsic properties of the fluid are key to interpreting microrheology experiments. Alternatively, the forces imposed on particles in a complex fluid can be used to manipulate the particles and arrange them into unique and useful structures (*3*–*6*).

Nematic liquid crystals are complex fluids possessing anisotropy that introduces both forces and torques on suspended particles (*7*–*17*). A nematic is composed of rod-like molecules and is characterized by an alignment of the long axes of the molecules along a particular direction. At an interface between a nematic and a surface, interactions between the surface and the liquid crystal molecules can create an energetically preferred orientation for the nematic alignment. For surfaces that are not flat, such as those of particles suspended in the nematic, these preferences can distort the otherwise uniform alignment, with a corresponding cost to the nematic's elastic energy. The tendency to minimize this energy can lead to forces on the particles. For example, recent studies on spherical particles that orient the nematic perpendicular to their surface have shown that the resulting distortions mediate interactions between the particles (*7*–*12*). However, few probes exist that can directly access such forces. Hence, despite their significance, few geometries exist for which quantitative information about them has been extracted (*8*, *12*, *18*), and the exploitation of these forces for manipulating particles remains largely unexplored. We have developed methods to manipulate anisotropic particles in nematic liquid crystals. The particles' shape introduces orientational degrees of freedom that lead to fluid-imposed forces and torques, which we have measured quantitatively. Specifically, by balancing the fluid-imposed forces on magnetic nanowires with either applied magnetic fields or gravity, we have determined the elastic torque on a wire and have measured a repulsion between a wire and a flat surface that is mediated by the nematic. As a demonstration of how these interactions can be controlled, we showed that a spatial variation in the nematic's alignment converts the torque into a translational force that can levitate a wire to a desired height.

In our experiments, isolated, highly cylindrical nickel wires 175 nm in radius (*19*) were contained in the room-temperature nematic liquid crystal pentylcyanobiphenol (5CB). The wire lengths ranged from 14 to 35 μm. The 5CB with nanowires was held between parallel glass plates, which were separated by 100 μm. The plates were coated with rubbed polyimide to create a uniform orientation for the nematic alignment parallel to the plates. Typically, one specifies the local alignment direction for a nematic by a

Department of Physics and Astronomy, Johns Hopkins University, Baltimore, MD 21218 USA.

vector **n**, called the director. Nematics are invariant under inversion of the director, **n** → –**n**, and their elastic energy is minimized when the orientation of **n** is spatially uniform. Polarization microscopy observations showed that the director at our wires' surfaces oriented parallel to the wires' long axis, a configuration known as longitudinal anchoring. Therefore, in equilibrium a wire orients with its long axis parallel to the director, as shown schematically in Fig. 1A. For a wire at some other orientation, as in Fig. 1B, the director must distort to satisfy this boundary condition. Such distortions increase the elastic energy U of the liquid crystal, and they consequently introduce a restoring torque that attempts to realign the wire with the director.

As a first step toward understanding the forces acting on anisotropic particles in nematics, we measured this elastic torque through microscopy observations. The samples were positioned on the stage of a Nikon TE2000 inverted microscope within a set of magnetic coils that produced magnetic fields of precisely controlled magnitude and direction within the microscope's focal plane. Images of the wires in the 5CB were made with a long-working-distance ×40 objective. Because the nickel wires possess a magnetic dipole moment μ parallel to their long axis, a small magnetic field β (in the range from 1 to 10 G) applied at an angle ϕ to the director rotates the wire to an angle θ with respect to the director, as in Fig. 1B (*20*). The wire comes to rest when the magnetic torque, $\mu B\sin(\phi - \theta)$, is balanced by the torque from the gradient in elastic energy

$$-\frac{\partial U}{\partial \theta} + \mu B\sin(\phi-\theta) = 0 \qquad (1)$$

Figure 1C shows results from measurements of $B\sin(\phi - \theta)$ versus θ for an isolated wire 14 μm long. The observed linear relation over an extended range of θ implies that the elastic energy grows quadratically with the angle of the wire; that is, $U \sim \theta^2$.

This result supports theoretical predictions based on the elastic energy of the nematic. In considering the behavior of an elongated inclusion in a nematic, Brochard and de Gennes (*15*) calculated this energy as a function of the inclusion's orientation. For the case of longitudinal anchoring, they exploited an analogy between the elastic energy of the nematic and the electrostatic field energy of an object at fixed potential to predict that the energy varies with particle orientation as

$$U = 2\pi CK\theta^2 \qquad (2)$$

where K is the Frank elastic constant of the nematic (*21*) within the approximation $K_{11} = K_{22} = K_{33} = K$ and $C \approx L/2\ln(L/2R)$ is the capacitance of a wire with length L and radius R (*22*). The θ^2 dependence in Eq. 2 is not derived from a small angle approximation but is analogous to the V^2 voltage dependence of the stored energy in a capacitor. The slope of the line in Fig. 1C, approximately 2.9 ± 0.1 G/radian, matches the expected value, $4\pi CK/\mu \approx 3$ G/radians, where $C \approx 2 \times 10^{-4}$ cm, $K \approx 5 \times 10^{-7}$ dynes (*23*), and $\mu/L \approx 3 \times 10^{-11}$ emu/μm (*24*), thus confirming quantitatively the validity of Eq. 2. This slope corresponds to a torque that grows with angle as 1×10^{-10} dyne cm/radian.

Although the symmetry of the nematic indicates that elastic distortions should be symmetric across $\theta = \pi/2$, the linear growth in the torque with θ extends to θ approaching π, as shown in Fig. 2A. However, applying a magnetic field that rotates the wire past $\theta = \pi$ causes an abrupt switch in the sign of the torque, so that θ goes from lagging ϕ to leading ϕ. After this switch, the torque again varies linearly with θ, with its magnitude crossing zero at $\theta = 2\pi$. A schematic diagram in Fig. 2B for the elastic energy illustrates this process. As the wire rotates past $\theta = \pi/2$, the director enters a metastable configuration as it remains on the energy branch, labeled I, with a minimum at $\theta = 0$. Transitions to the equilibrium director configuration corresponding to branch II are suppressed. At $\theta = \pi$, the director switches from the configuration of branch I to a different metastable configuration corresponding to branch III, ultimately reaching a distortion-free configuration at $\theta = 2\pi$.

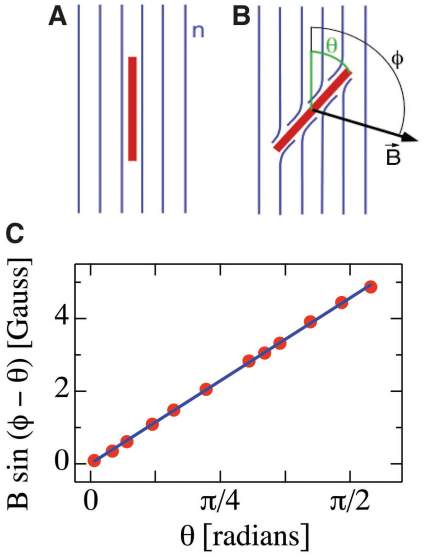

Fig. 1. Orientation-dependent elastic torque on a nickel nanowire with longitudinal anchoring in the nematic liquid crystal 5CB. (**A**) In equilibrium, the wire (red) orients parallel to the nematic director (blue). (**B**) When a magnetic field is introduced, the wire reorients, leading to a distortion of the director near the wire. The wire comes to rest at an angle θ when the magnetic torque and elastic torque balance. (**C**) The results for the torque as a function of θ for a 14-μm-long wire display a characteristic linear dependence that corresponds to quadratic growth in elastic energy with angle, $U \sim \theta^2$.

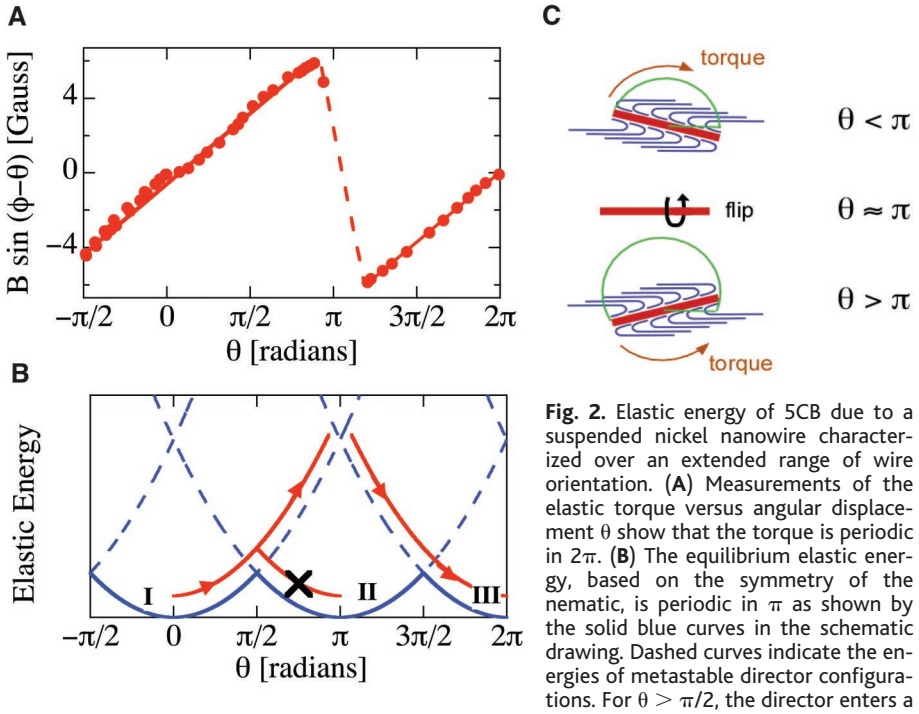

Fig. 2. Elastic energy of 5CB due to a suspended nickel nanowire characterized over an extended range of wire orientation. (**A**) Measurements of the elastic torque versus angular displacement θ show that the torque is periodic in 2π. (**B**) The equilibrium elastic energy, based on the symmetry of the nematic, is periodic in π as shown by the solid blue curves in the schematic drawing. Dashed curves indicate the energies of metastable director configurations. For $\theta > \pi/2$, the director enters a metastable configuration and follows the red arrows. Changes in the director that maintain an equilibrium configuration are suppressed, as indicated by the black cross. (**C**) Movies of the crossover from energy branch I to energy branch III show that the wire spins about its long axis by 180° as θ crosses π, as indicated in the pictures here.

Movies tracking the change from branch I to branch III show that during the transition, the wire spins about its long axis by 180°. (This effect can be seen very clearly for wires that are slightly bent.) Schematic pictures of the nematic distortions, shown in Fig. 2C, indicate how flipping the wire in this way can facilitate the transition. The director field in the rotation plane remains unchanged with respect to the wire before and after the flip, suggesting that no intermediate configurations with prohibitively large energy must be traversed to move between branches I and III. In contrast, switching between branches I and II requires the nucleation of a disclination line (*15*) whose energy makes such transitions generally unfeasible. Although the diagrams in Fig. 2C provide a sense of the transition from branch I to III, an interesting question remains as to how the nematic imparts angular momentum to the wire parallel to its long axis to cause the flip. A mapping of the full three-dimensional director field would be needed to clarify this issue.

Beyond the torques characterized in Figs. 1 and 2, orientation-dependent nematic distortions can generate interactions between a wire and other objects. For example, because of the longitudinal anchoring at the wire surface and the parallel orientation of the director at the glass plates resulting from the rubbed polyimide, a wire that rotates away from $\theta = 0$ near a plate will introduce a twist in the director concentrated between the underside of the wire and the plate. Following the electrostatic analogy introduced by Brochard and de Gennes, this geometry maps to the problem of a wire at fixed voltage lying parallel to a plane held at a different voltage. The capacitance per unit of length in this electrostatic problem decreases with increasing separation of wire and plane, leading to a repulsive force between them (*16*). We have observed that sedimented wires rotated by a magnetic field rise off the bottom glass surface, demonstrating the existence of a corresponding repulsion in the liquid crystal system. Figure 3 displays results for the equilibrium height above the bottom plate reached by a wire when the elastic forces on it are balanced by gravity. In the measurement, the wire, 24 μm long, is held between glass surfaces with a separation of 80 μm. The dashed line in the figure is the relation between θ and the wire's height z expected based on a balance of gravity and the repulsive force from a single surface (*16*)

$$\theta^2 = \frac{\delta Mg}{K\pi}\sqrt{1-(R/z)^2}\,[\sec h^{-1}(R/z)]^2 z \qquad (3)$$

where g is the gravitational constant and $\delta M = \pi R^2 L(\rho_{Ni} - \rho_n)$ is the effective mass of the nickel wire with density ρ_{Ni} in 5CB with density ρ_n. With increasing height, repulsion between the wire and the top glass plate becomes increasingly important. To approximate this effect, we model the balance of the gravitational force on the wire, $\delta Mg = 2 \times 10^{-8}$ dynes, with a superposition of the repulsive forces from top and bottom surfaces as determined separately using Eq. 3. The solid line in Fig. 3 is the result of a fit to this form (*25*).

We note that the interaction between a wire and a plate implies not only a repulsive force when $\theta > 0$, but a torque that tries to restore θ to 0. We have found that the magnitude of this torque grows quickly as a wire approaches within roughly 5 μm of a plate. At larger heights, the torque becomes independent of height to within the precision of our measurements. The results of torque on a wire presented in Figs. 1 and 2 were obtained on wires lifted by the repulsive force to large heights, so that the experimental conditions best approximated those of a wire in a bulk nematic, as considered by Brochard and de Gennes (*15*).

The orientation-dependent elastic energy of an anisotropic particle suspended in a nematic can be exploited to manipulate the particles via judiciously designed spatial variations in the director orientation. Figure 4A shows a schematic of a twisted nematic in which a nickel nanowire is made neutrally buoyant. The upper and lower plates of the cell are treated so that the director aligns parallel to each surface but at orientations that are offset from each other by π/2. The director within the cell thus twists through an angle of π/2 with a uniform pitch to match both boundary conditions. When a large magnetic field ($B \approx 50$ G) is applied so that a wire aligns parallel with the field, the elastic energy becomes a function of the wire's height. Following Eq. 2, a wire near the bottom of the cell feels an "elastic lift"

$$F_z = -\frac{\partial U}{\partial z} = 4\pi KC\left(\frac{\partial \theta}{\partial z}\right)^2 (z_0 - z) \qquad (4)$$

where z_0 is the height at which the field is parallel to the local director and $\partial\theta/\partial z$ is the magnitude of the twist. This lift can easily reverse the sedimentation of wires by gravity. Figure 4B shows results for the height of a wire 35 μm long as a function of time as it rises in a twisted cell with total thickness of 100 μm for three different values of z_0. Assuming the lift is countered by gravity and a viscous drag, the equation of motion for the wire is

$$4\pi KC\left(\frac{\partial \theta}{\partial z}\right)^2 (z_0 - z) - \delta Mg - \Gamma \dot{z} = 0 \qquad (5)$$

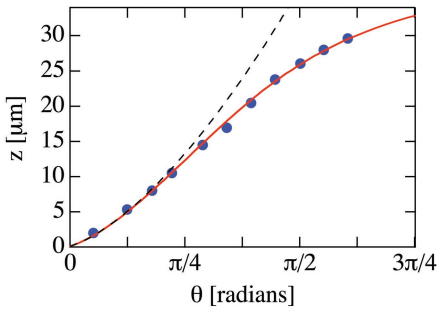

Fig. 3. Orientation-dependent repulsion of a nanowire by flat surfaces with planar anchoring. The solid circles mark the height of a wire from the bottom surface, z, as a function of θ when the elastic forces and gravitational force on the wire balance. The dashed line denotes the relation between z and θ expected when only the repulsion from the bottom surface is considered, as given by Eq. 3. The solid line is the result of a fit in which a repulsion from the top surface is superposed on the repulsion from the bottom surface (*25*).

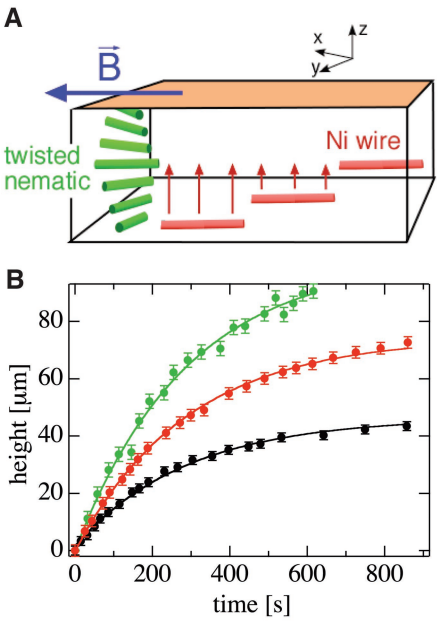

Fig. 4. Levitation of a nickel wire within a twisted nematic. (**A**) The director in the experiment, denoted in green, twists uniformly as a function of height to match the directions of planar anchoring at the upper and lower surfaces (along $\hat{x}$ and $\hat{y}$, respectively). When a magnetic field aligns a wire parallel to the director at some height in the cell (such as at the center of the cell in the figure), the elastic energy becomes a function of the wire's height, leading to a levitating force on a wire resting on the bottom substrate. (**B**) Measurements demonstrate that the height of a wire initially resting at the bottom rises as a function of time in response to this force. Results are shown for three sets of measurements corresponding to rotations of the wire to different orientations in 100-μm-thick 5CB. For the green data set, the wire's angle of rotation exceeds the director orientation at the top surface, so that the wire rises until it reaches this surface. The solid lines are results of fits to Eq. 6.

where $\Gamma = 4\pi\eta L/[\ln(L/2R) + 0.84]$ is the Stokes drag coefficient for a cylinder (*26*), and η is the effective viscosity of the nematic. The solid lines in Fig. 4B are the results of fits to the solution of this equation

$$z(t) = \left(z_0 - \frac{\delta Mg}{4\,\pi KC(\partial\theta/\partial z)^2}\right)[1 - exp(-t/\tau)] \quad (6)$$

with the time constant, $\tau = \Gamma/[4\pi KC(\partial\theta/\partial z)^2]$, constrained to have the same value, $\tau = 270$ s, in all three fits. These results give clear qualitative support for Eqs. 4 to 6 in describing the levitation. Quantitative comparisons are made difficult by the complicated anisotropy of the nematic's viscoelasticity (*21*). However, selecting characteristic values for 5CB of $\eta \sim 1$ Poise (*27*) and $K \approx 5 \times 10^{-7}$ dynes leads to $\tau \approx 140$ s, which is in reasonable agreement with the measured value.

This manipulation of wires with director gradients suggests methods for self-assembly using more elaborate spatially dependent director fields. For example, as a straightforward extension of the levitation, a liquid crystal that twists through many periods (such as a cholesteric liquid crystal) could serve as host to the creation of a periodic array of planes of oriented nanowires. Another possible application of these forces involves wire sorting through the repulsion from a flat surface. As Eq. 3 indicates, gravity and the repulsive force balance at a height that varies to first order with R^{-2} and is independent of L when θ is fixed; for example, by a large external field. Hence this repulsion can be used to spatially separate wires of different radii.

References and Notes

1. W. B. Russel, D. A. Saville, W. R. Schowalter, *Colloidal Dispersions* (Cambridge Univ. Press, Cambridge, 1989).
2. F. C. MacKintosh, C. F. Schmidt, *Curr. Opin. Colloid Interface Sci.* **4**, 300 (1999).
3. T. L. Morkved, P. Wiltzius, H. M. Jaeger, D. G. Grier, T. A. Witten, *Appl. Phys. Lett.* **64**, 422 (1994).
4. R. B. Thompson, V. V. Ginzburg, M. W. Matsen, *Science* **292**, 2469 (2001).
5. K. Shin *et al.*, *Nano Lett.* **2**, 933 (2002).
6. N. Bowden, A. Terfort, J. Carbeck, G. M. Whitesides, *Science* **276**, 233 (1997).
7. P. Poulin, H. Stark, T. C. Lubensky, D. A. Weitz, *Science* **275**, 1770 (1997).
8. P. Poulin, V. Cabuil, D. A. Weitz, *Phys. Rev. Lett.* **79**, 4862 (1997).
9. T. C. Lubensky, D. Pettey, N. Currier, H. Stark, *Phys. Rev. E* **57**, 610 (1998).
10. O. Mondain-Monval, J. C. Dedieu, T. Gulik-Krzywicki, P. Poulin, *Eur. Phys. J. B* **12**, 167 (1999).
11. J.-C. Loudet, P. Barois, P. Poulin, *Nature* **407**, 611 (2000).
12. J. C. Loudet, P. Poulin, *Phys. Rev. Lett.* **87**, 165503 (2001).
13. J.-I. Fukuda, B. I. Lev, K. M. Aoki, H. Yokoyama, *Phys. Rev. E* **66**, 051711 (2002).
14. M. Tasinkevych, N. M. Silvestre, P. Patricio, M. M. Telo de Gama, *Eur. Phys. J. E* **9**, 341 (2002).
15. F. Brochard, P. G de Gennes, *J. Phys.* (*Paris*) **31**, 691 (1970).
16. F. Alouges, B. D. Coleman, *J. Phys. A Math. Gen.* **32**, 1177 (1999).
17. D. Andrienko, M. P. Allen, G. Skacej, S. Zumer, *Phys. Rev. E* **65**, 041702 (2002).
18. A. B. Bracic, K. Kocevar, I. Musevic, S. Zumer, *Phys. Rev. E* **68**, 011708 (2003).
19. The nickel wires were fabricated via electrodeposition into nanoporous alumina templates [M. Tanase *et al.*, *Nano Lett.* **1**, 155 (2001)].
20. The sizes of the applied magnetic fields are several orders of magnitude smaller than those required to reorient the nematic director because of its magnetic anisotropy.
21. P. G. de Gennes, J. Prost, *The Physics of Liquid Crystals* (Oxford Univ. Press, Oxford, 1993).
22. This expression for the capacitance is for an ellipsoid and therefore is only approximate for the case of a cylinder.
23. N. V. Madhusudana, R. Pratibha, *Mol. Cryst. Liq. Cryst.* **89**, 249 (1982).
24. A. Hultgren, M. Tanase, C. S. Chen, G. J. Meyer, D. H. Reich, *J. Appl. Phys.* **43**, 7554 (2003).
25. The height based on a superposition of two elastic forces is only an approximate solution. The exact solution requires solving the boundary value problem that accounts for all three surfaces (wire and two planes) simultaneously.
26. M. M. Tirado, J. G. de la Torre, *J. Chem. Phys.* **71**, 2581 (1979).
27. A. G. Chmielewski, *Mol. Cryst. Liq. Cryst.* **132**, 339 (1986).

28. We thank C. Denniston and J. Harden for helpful discussions and M. Tanase for assistance with wire synthesis. Funding was provided by NSF through grants DMR-0134377 and DMR-0080031.

15 October 2003; accepted 11 December 2003

Local Gate Control of a Carbon Nanotube Double Quantum Dot

N. Mason,*† M. J. Biercuk,* C. M. Marcus†

We have measured carbon nanotube quantum dots with multiple electrostatic gates and used the resulting enhanced control to investigate a nanotube double quantum dot. Transport measurements reveal honeycomb charge stability diagrams as a function of two nearly independent gate voltages. The device can be tuned from weak to strong interdot tunnel-coupling regimes, and the transparency of the leads can be controlled independently. We extract values of energy-level spacings, capacitances, and interaction energies for this system. This ability to control electron interactions in the quantum regime in a molecular conductor is important for applications such as quantum computation.

Carbon nanotubes have been considered leading candidates for nanoscale electronic applications (*1*, *2*). Previous measurements of nanotube electronics have shown electron confinement (quantum dot) effects such as single-electron charging and energy-level quantization (*3*–*5*). Nanotube properties such as long spin lifetimes make them ideal candidates for spin-based quantum computation based on double quantum dots (*6*) or multiple series quantum dots (*7*). However, realizing such devices requires independent gate control over multiple charges and spins. This ability has not been achieved in previous measurements, where device properties were controlled with a single global gate such as the doped silicon substrate (*8*–*10*). We report the fabrication and measurement of a nanotube-based double quantum dot with multiple, independent gates. The gates are used to manipulate and study single-electron charging as well as charge interactions, and relevant device parameters are extracted directly from transport data.

Department of Physics, Harvard University Cambridge, MA 02138, USA.

*These authors contributed equally to this work.
†To whom correspondence should be addressed. E-mail: marcus@harvard.edu (C.M.M.); nmason@fas.harvard.edu (N.M.)

The device under study consists of a nanotube ~2 nm in diameter, of length $L \sim 1.5$ μm between metal contacts, with three top gates (*11*, *12*) and a doped Si backgate (Fig. 1) (*13*). Room temperature measurements of conductance as a function of any gate voltage indicate either that the nanotube is metallic with a strong resonance or that it is a small band-gap semiconductor. At low temperatures, single-electron charging is observed as Coulomb blockade conductance peaks, measured as a function of applied gate voltages. The observed peak pattern is different for each gate and in some regions shows considerable superstructure, which appears with increasing source-drain voltage, V_{SD}. We observe a double periodicity of Coulomb charging phenomena, which is consistent with a nanotube quantum dot, defined by tunnel barriers to the leads, that has been split into two dots of roughly equal size by a defect in the middle of the device (*14*). Structural defects often create tunable tunnel barriers (*15*–*18*) and typically appear in nanotubes longer than ~200 nm. Although such defects can be controllably fabricated (*19*), in this case the defect is inherent to the tube. The resulting dots each have a quantized energy level spacing of $\Delta = h\nu_F/2L \sim 1$ meV (assuming only spin degeneracy), where $\nu_F = 8.1 \times 10^5$ m/s is the Fermi velocity for a metallic nanotube (*4*).

The top gate voltages have differential capacitive coupling to the quantized energy levels of the two dots. Transport measurements indi-